Recent Results from the ANTARES Neutrino Telescope

S. MANGANO, on behalf of the ANTARES Collaboration
IFIC - Instituto de Física Corpuscular, Polígono de la Coma, 46980 Paterna, Spain

The ANTARES experiment is currently the largest underwater neutrino telescope. It is taking high quality data since 2007 and aims to detect high energy neutrinos that are expected from the acceleration of cosmic rays from astrophysical sources. We will review the status of the detector and present several analyses carried out on atmospheric muons and neutrinos. For example we will show the latest results from searches for neutrinos from steady cosmic point-like sources, for neutrinos from Fermi Bubbles, for neutrinos from Dark Matter in the Sun and the measurement of atmospheric neutrino oscillation parameters.

1 Introduction

The discovery of high energy cosmic rays which collide with the Earth's atmosphere is known since 100 years, but their astrophysical origin and their acceleration to such high energies is still unclear. The observation of these cosmic rays is a strong argument for the existence of high energy neutrinos from the cosmos. Such cosmic neutrinos are expected to be emitted along with gamma-rays by astrophysical sources in processes involving the interaction of accelerated hadrons and the subsequent production and decay of pions and kaons.

The advantage of using neutrinos with respect to cosmic particles like protons and photons is that they are not deflected by magnetic fields and are weakly interacting. The neutrinos point directly back to the source of emission and can provide information about the source.

The disadvantage to detecting neutrinos is their extremely small interaction probability. A very large amount of matter is needed to have some interacting neutrinos. The flux of high energy cosmic neutrinos can be estimated from the observation of the rate of high energy cosmic rays. Theoretical calculations show that a detector of the size of about a cubic kilometer is needed to discover high energy cosmic neutrinos.

A cost effective way to detect high energies neutrinos is to use detector material found in nature, like water and ice. The detector material has to be equipped by a three dimensional array of light sensors, so that muon neutrinos are identified by the muons that are produced in charged current interactions. These muons are detected by measuring the Cerenkov light which they emit when charged particles move faster than the speed of light in the detector material. The knowledge of the timing of the Cerenkov light recorded by the light sensors allows to reconstruct the trajectory of the muon and so to infer the arrival direction of the incident neutrino. This technique is used in large-scale Cerenkov detectors like IceCube [1] and ANTARES [2] which are currently looking for high-energy (~TeV and beyond) cosmic neutrinos.

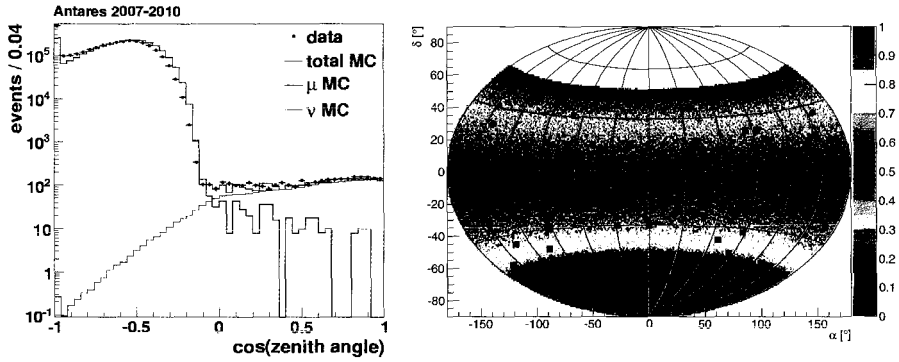

Figure 1: *Left: The reconstructed zenith angle data distribution of selected events compared to the Monte Carlo distribution for atmospheric neutrino and muon background. Right: Skymap in equatorial coordinates of the 51 neutrino candidate sources (blue squares) and the 11 most promising gravitational lensing systems (black circles). The ANTARES visibility is also shown.*

2 ANTARES Neutrino Telescope

The ANTARES detector is taking data since the first lines were deployed in 2007. It is located in the Mediterranean Sea, 40 km off the French coast at 42°50′N, 6°10′E. The detector consists of twelve vertical lines equipped with 885 photomultipliers (PMTs) in total, installed at a depth of about 2.5 km. The distance between adjacent lines is of the order of about 70 m. Each line is equipped with up to 25 triplets of PMTs spaced vertically by 14.5 m. The PMTs are oriented with their axis pointing downwards at 45° from the vertical. The instrumented detector volume is about 0.02 km^3. The design of ANTARES is optimized for the detection of upward going muons produced by neutrinos which have traversed the Earth, in order to limit the background from downward going atmospheric muons. The instantaneous field of view is 2π sr for neutrino energies between 10 GeV and 100 TeV, due to selection of upgoing events. Further details on the detector can be found elsewhere [2].

3 Cosmic Point-Like Neutrino Sources

The main goal of the ANTARES neutrino telescope is the observation of neutrinos of cosmic origin in the Southern sky. The main physical background to identify cosmic neutrinos are atmospheric muons and upward going atmospheric neutrinos. The atmospheric muons are produced in the upper atmosphere by the interaction of cosmic rays and can reach the apparatus despite the shielding provided by 2 km of water. Figure 1 left shows a comparison of the zenith angle distribution between data and Monte Carlo simulation. It can be seen that the flux of atmospheric muons is several order of magnitude larger than that of atmospheric neutrinos and that there is a good agreement between data and the Monte Carlo simulation.

The collaboration has developed several strategies to search in its data either for diffuse [3] or point-like [4,5] cosmic neutrino sources, possibly in association with other cosmic messengers such as gamma-rays [6,7] or gravitational waves [8]. Clustering of neutrino arrival directions can provide hints for their astrophysical origin. In the search of cosmic neutrino point sources, upward going events have been selected in order to reject atmospheric muons. Additional cuts on the quality of the muon track reconstruction have been applied in order to eliminate events that correspond to downward going atmospheric muons which are misreconstructed as upward going. Most of

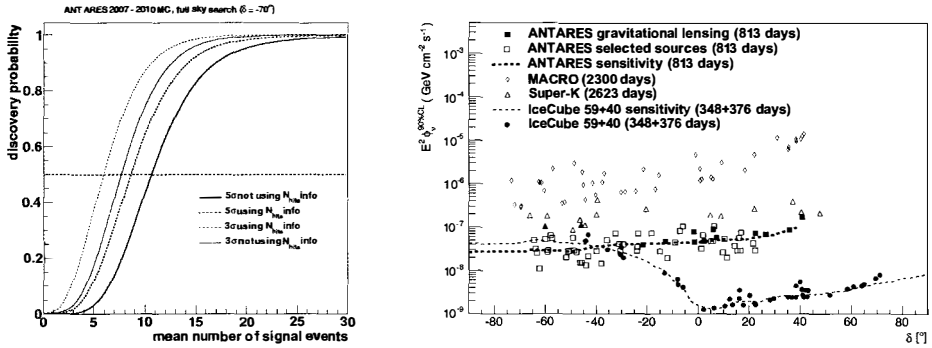

Figure 2: *Left: Probability for a 3 (red lines) and 5 (blue lines) sigma discovery as a function of the mean number of signal events. The dashed lines show the case where the number of hits information is used as an energy estimator in the likelihood, whereas for the solid lines no energy information is used. Right: Upper limits (at 90% C.L.) on the E^{-2} neutrino flux from the 62 selected candidate sources as well as the sensitivity as function of the declination. Also shown are the results from other experiments.*

the remaining events are atmospheric muon neutrinos which constitute an irreducible diffuse background for cosmic neutrino searches. The 2007-2010 data contain around 3000 neutrino candidates with a predicted atmospheric muon neutrino purity of around 85%. The estimated angular resolution is 0.5±0.1 degrees.

The selection criteria are optimized to search for E^{-2} neutrino flux from point-like astrophysical sources, following two different strategies: a full sky search and a search in the direction of particularly interesting neutrino candidate sources. The selection of these sources is either based on the intensity of their gamma-ray emission as observed by Fermi [9] and HESS [10] or based on strong gravitational lensed sources with large magnification.

The motivation to select lensed sources is that neutrino fluxes as photon fluxes can be enhanced by the gravitational lensing effect, which could allow to observe sources otherwise below the detection threshold. Neutrinos (contrary to photons) are not absorbed by the gravitational lens. Therefore, sources with a moderate observed gamma-ray flux could be interesting candidates for neutrino telescopes. Figure 1 right shows the skymap in equatorial coordinates with the ANTARES visibility of the 51 neutrino candidate sources with strong gamma-ray emission and the 11 most promising strong gravitationally lensed sources.

The cosmic point source search has been performed using an unbinned maximum likelihood method [5]. This method uses the information of the event direction and, since the cosmic sources are expected to have a much harder spectra than atmospheric neutrinos, the number of hits produced by the track. Figure 2 left shows how the introduction of an energy estimator like the number of hits increases the discovery potential about 25% in comparison without using such an information. For each source, the position of the cluster is fixed at the direction of the source and the likelihood function is maximized with respect to the number of signal events. In the absence of a significant excess of neutrinos above an expected background, an upper limit on the neutrino flux is calculated.

A full sky point source search based on the above mentioned algorithm has not revealed a significant excess for any direction. The most significant cluster of events in the full sky search, with a post-trial p-value of 2.6%, which is equivalent to 2.2σ, corresponds to the location of $(\alpha, \delta) = (-46.5°, 65.0°)$. No significant excess has been found also in the dedicated search from the list of 11 lensed and 51 gamma-rays selected neutrino source candidates. The obtained neutrino flux limits of these selected directions are plotted as function of declination in Figure 2

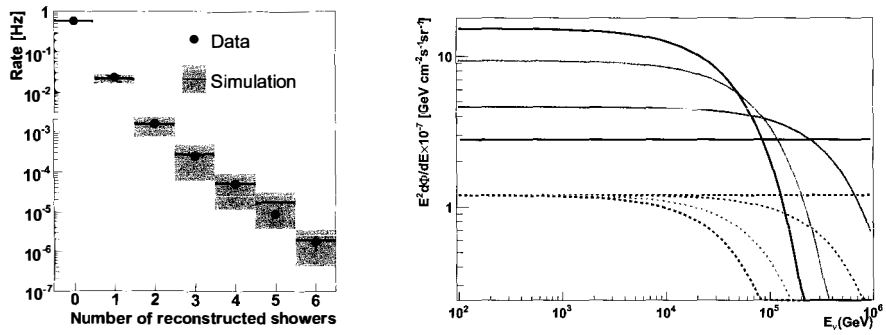

Figure 3: *Left: Muon event rate as a function of the shower multiplicity for data (points) and the Corsika simulation (line). The systematic error for the simulation is given by the height of the gray bands. Only statistical errors are shown for the data points. Right: Upper limits (at 90% C.L.) on the E^{-2} neutrino flux from the Fermi Bubbles for different cutoffs: no cutoff (black), 500 TeV (red), 100 TeV (green), 50 TeV (blue) are shown together with theoretical predictions in case of pure hadronic model (dashed lines).*

right, where for comparison the limits set by other neutrino experiments is also shown.

4 Electromagnetic Showers along Muon Tracks

Even if the primary aim of ANTARES is the detection of high energy cosmic neutrinos, the detector measures mainly downward going muons. These muons are the decay products of cosmic ray collisions in the Earth's atmosphere. Atmospheric muon data have been used for several analyses [11,12,13], in particular the collaboration investigated the sensitivity of the composition of cosmic rays through the downward going muon flux [14]. Several observational parameters are combined to estimate the relative contribution of light and heavy cosmic rays. One of these parameters is the number of electromagnetic showers along muon tracks.

Catastrophic energy losses appear occasionally, when a high energy muon (~ 1 TeV) traverses the water. These energy losses are characterized by discrete bursts of Cerenkov light originating mostly from pair production and bremsstrahlung (electromagnetic showers). A shower identification algorithm [15,16] is used to identify the excess of photons above the continuous baseline of photons emitted by a minimum-ionizing muon. With this method downward going muons with energies up to 100 TeV have been analysed.

The muon event rate as a function of the number of identified showers is plotted in Figure 3 left. The distribution shows the results for data and a Corsika based simulation. As can be seen, about 5% of the selected muon tracks have at least one well identified shower. Also shown is the systematic uncertainty for the simulation, where the largest systematic errors arises from uncertainties on the PMT angular acceptance and absorption length.

5 Fermi Bubbles

The Fermi Satellite has revealed an excess of gamma-rays in an extended pair of bilateral bubbles above and below our Galactic Center. These so called Fermi Bubbles (FB) cover about 0.8 sr of the sky, have sharp edges, are relative constant in intensity and have a flat E^{-2} spectrum between 1 and 100 GeV.

It has been proposed that FB are seen due to cosmic ray interactions with the interstellar medium, which produce pions. In this scenario gamma rays and high-energy neutrino emission

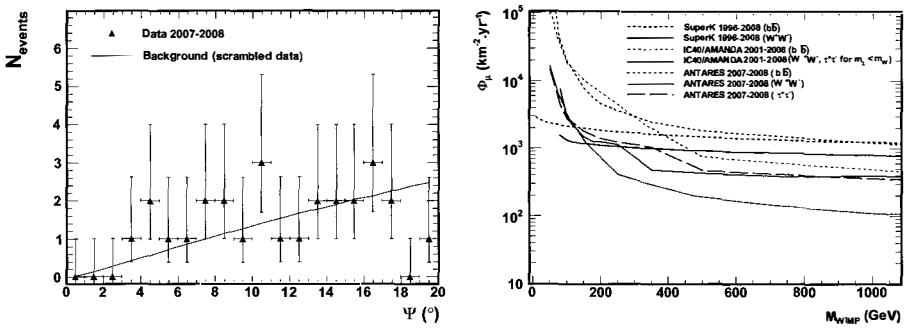

Figure 4: *Left: The number of observed neutrinos (black triangles) and expected background events (solid blue line) as a function of the search cone radius around the Sun. A 1σ Poisson uncertainty is shown for each data point. Right: 90% C.L. upper limit on the muon flux as a function of the WIMP mass for three self-annihilation channels $b\bar{b}$ (dotted line), W^+W^- (solid line) and $\tau^+\tau^-$ (dashed line). The results from Super-Kamiokande (in blue) and IceCube (in green) are also shown.*

are expected with a similar flux from the pions decay.

ANTARES has an excellent visibility to the FB and therefore a dedicated search for an excess of neutrinos in the region of FB has been performed [17]. This analysis compares the rate of observed neutrino events in the region of the FB to that observed excluding the FB region. The of source FB region is equivalent in size and has in average the same detector efficiency as the FB region. The analyzed 2008-2011 data reveal 16 neutrino events inside the FB region. Estimations from outside the FB region predicts 11 neutrino events. These results are compatible with no signal and limits are placed on the fluxes of neutrinos for various assumptions on the energy cutoff at the source. Figure 3 right shows the upper limits and compares it to expected signal for optimistic models [18]. It can be seen that the calculated upper limits are within a factor 3 above the expected signal.

6 Dark Matter

The indirect search for dark matter in the universe is one further goal of ANTARES [19]. The weakly interactive massive particles could be gravitationally trapped in the center of the Sun. After the self-annihilation process of these weakly interactive massive particles neutrinos can be created.

Using the data recorded during 2007 and 2008, a search for high energy neutrinos coming from the direction of the Sun has been performed. The neutrino selection criteria have been chosen to maximize a possible neutrino signal. Decay channels leading to both hard ($W^+W^-, \tau^+\tau^-$) and soft ($b\bar{b}$) flux spectra are considered. The expected background is estimated from the data by scrambling the direction of the observed neutrino candidates. The number of events in a search cone around the Sun is shown in Figure 4 left as a function of the search cone radius. It can be seen that the number of observed neutrino candidates is in good agreement with the background expectations. As there is no evidence for a flux of neutrinos from the Sun, upper limits on the muon flux are set and are presented in Figure 4 right. For comparison the limits from the other experiments such as IceCube [20] and Super-Kamiokande [21] are also shown. By improving the event selection and including data already available the analysis can be improved by around an order of magnitude.

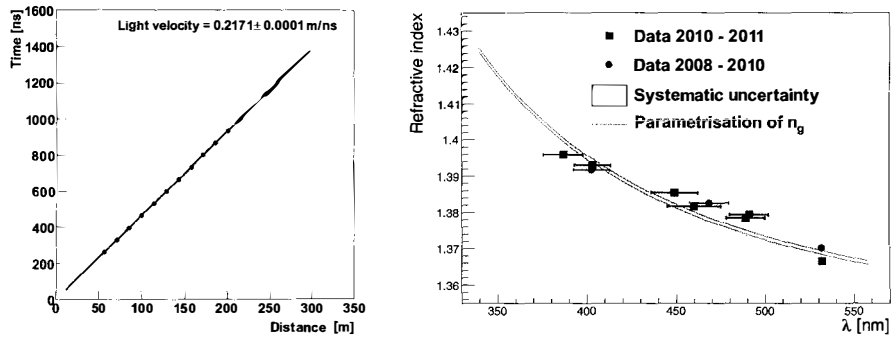

Figure 5: *Left: Arrival time as a function of the distance between the LED ($\lambda = 469$ nm) and the PMT. The solid line corresponds to a fit of a linear function to the data. Right: Index of refraction corresponding to the group velocity of light as a function of the wavelength. The gray band shows the systematic uncertainty. The two solid lines correspond to a parametrization of the index of refraction evaluated at a pressure of 200 atm (lower line) and 240 atm (upper line).*

7 Velocity of Light in Water

Charged particles crossing sea water induce the emission of Cerenkov light whenever the condition $\beta > 1/n_p$ is fulfilled, where β is the speed of the particle relative to the speed of light in vacuum and n_p is the phase refractive index. The Cerenkov photons are emitted at an angle with respect to the particle track given by $\cos\theta_c = \frac{1}{\beta n_p}$. The individual photons then travel in the medium at the group velocity. Both the phase and group refractive indices depend on the wavelength of the photons and has the effect of making the emission angle and the speed of light wavelength dependent. Good knowledge of this wavelength dependence enables to reach the optimal performance of the detector.

The velocity of light has been measured using a set of pulsed light sources (LEDs emitting at different wavelengths) distributed throughout the detector illuminating the PMTs through the water[22]. In special calibration data runs the emission time and the position of the isotropic light flash, as well as the arrival time and the position when the light reaches the PMTs are recorded. Figure 5 left shows the arrival time as a function of the distance between the LED and the different PMTs. The slope of a linear fit to the arrival time versus distance gives the inverse of the light velocity. The refractive index has been measured at eight different wavelengths between 385 nm and 532 nm. This refractive index with its systematic errors are shown in Figure 5 right. Also shown is the parametric formula of the refractive index. The measurements are in agreement with the parametrization of the group refractive index.

8 Atmospheric Neutrino Oscillations

ANTARES is also sensitive to neutrino oscillation parameters through the disappearance of atmospheric muon neutrinos[23].

Neutrino oscillation are commonly described in terms of L/E, where L the oscillation path length and E is the neutrino energy. For upward going neutrinos crossing the Earth the travel distance L is translated to $D\cos\theta$ where D is the Earth diameter and θ the zenith angle. Within the two-flavour approximation, the ν_μ survival probability can be written as

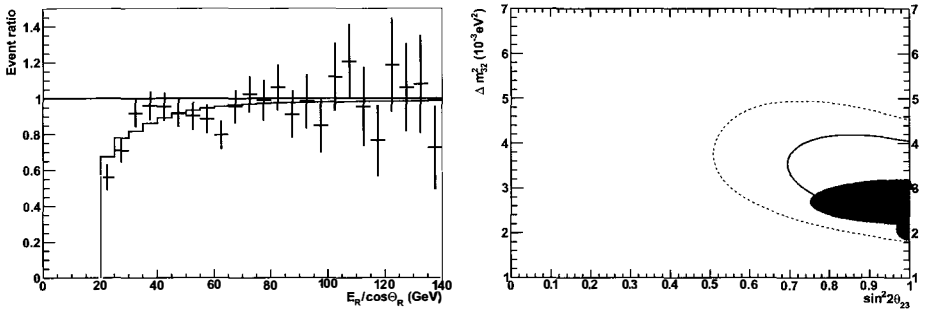

Figure 6: *Left: The fraction of events as a function of the $E_R/cos\theta_R$ distribution. Black crosses are data with statistical uncertainties, the blue histogram shows the non-oscillation hypothesis and the red histogram shows the result of the best fit. Right: 68% and 90% C.L. contours (solid and dashed red lines) of the neutrino oscillation parameters as derived from the fit of the $E_R/cos\theta_R$ distribution. The best fit point is indicated by the triangle. For comparison the solid filled regions show results at 68% C.L. from K2K (green), MINOS (blue) and Super-Kamiokande (magenta).*

$$P(\nu_\mu \to \nu_\mu) = 1 - \sin^2 2\theta_{23} \cdot \sin^2(1.27 \triangle m^2_{23} \frac{L}{E_\nu}) = 1 - \sin^2 2\theta_{23} \cdot \sin^2(16200 \triangle m^2_{23} \frac{\cos\theta}{E_\nu}),$$

where θ_{23} is the mixing angle and $\triangle m^2_{23}$ is the squared mass difference of the mass eigenstates (with L in km, E_ν in GeV and $\triangle m^2_{23}$ in eV^2). The survival probability P depends only on the two oscillation parameters, $sin^2 2\theta_{23}$ and $\triangle m^2_{23}$, which determine the behavior for the atmospheric neutrino oscillations.

Taking the recent results from the MINOS experiment [24], the first minimum in the muon neutrino survival probability ($P(\nu_\mu \to \nu_\mu) = 0$) occurs for vertical upward going neutrinos at about 24 GeV. Muons induced by a 24 GeV neutrino travel in average around 120 m in sea water. The detector has PMTs spaced vertically by 14.5 m so that this energy range can be reached for events detected on one single line.

The reconstructed flight path through the Earth is reconstructed through zenith angle θ_R, which is estimated from a muon track fit [25]. Whereas the neutrino energy E_R is estimated from the observed muon range in the detector. Figure 6 left shows event rate of the the measured variable $E_R/cos\theta_R$ for a data sample from 2007 to 2010 with a total live time of 863 days. The neutrino oscillations causes a clear event suppression for $E_R/cos\theta_R < 60GeV$ with a clean sample of atmospheric neutrinos with energies as low as 20 GeV. The parameters of the atmospheric neutrino oscillations are extracted by fitting the event rate as a function $E_R/cos\theta_R$ and is plotted as a red curve in Figure 6 left with values $\triangle m^2_{23} = 3.1 \cdot 10^{-3} eV^2$ and $sin^2 2\theta_{23} = 1$.

This measurement is converted into limits of the oscillation parameters and is shown in Figure 6 right. If maximum mixing is imposed ($sin^2 2\theta_{23} = 1$) the values of $\triangle m^2_{23}$ is $\triangle m^2_{23} = (3.1 \pm 0.9) \cdot 10^{-3} eV^2$. This measurement is in good agreement with the world average measurements. Although the results are not competitive with dedicated experiments, the ANTARES detector demonstrates the capability to measure atmospheric neutrino oscillation parameters and to detect and measure energies as low as 20 GeV.

9 Conclusion

ANTARES has been taking data since the first lines were deployed in 2007. With these data a broad physics program is underway producing competitive results. Unfortunately ANTARES has still not seen any cosmic neutrinos.

In this proceeding there was not enough room to discuss other topics which were illustrated at the Rencontres de Moriond, such as the atmospheric muon [11] and neutrino fluxes [3], the time calibration system [26], the acoustic neutrino detection system [27], the search for relativistic magnetic monopoles [28], the searches for nuclearites [29] and the correlation of neutrinos with gravitational waves [8], for which the reader is referred to elsewhere.

Neutrino telescopes are starting to open up a new window in the sky exploring new territory and they will hopefully reveal new unknown phenomena and help answer open questions.

Acknowledgments

I gratefully acknowledge the support of the JAE-Doc postdoctoral program of CSIC. This work has also been supported by the following Spanish projects: FPA2009-13983-C02-01, MultiDark Consolider CSD2009-00064, ACI2009-1020 of MICINN and Prometeo/2009/026 of Generalitat Valenciana.

References

1. A. Achterberg *et al*, *Astropart. Phys.* **26**, 155 (2006).
2. M. Ageron *et al*, *Nucl. Instrum. Methods* A **656**, 11 (2011).
3. J.A. Aguilar *et al*, *Phys. Lett.* B **696**, 16 (2011).
4. S. Adrian-Martinez *et al*, *Astrophys. J. Lett.* **743**, L14 (2011).
5. S. Adrian-Martinez *et al*, *Astrophys. J.* **760**, 53 (2012).
6. S. Adrian-Martinez *et al*, *JCAP* **1303**, 006 (2013).
7. S. Adrian-Martinez *et al*, *Astropart. Phys.* **36**, 634 (2012).
8. S. Adrian-Martinez *et al*, arXiv:1205.3018, accepted by JCAP (2012).
9. W.B. Atwood *et al*, *Astrophys. J.* **697**, 1071 (2009).
10. K. Bernloehr *et al*, *Astropart. Phys.* **20**, 111 (2003).
11. J.A. Aguilar *et al*, *Astropart. Phys.* **33**, 86 (2010).
12. S. Mangano *et al*, arXiv:0908.0858 (2009).
13. J.A. Aguilar *et al*, *Astropart. Phys.* **34**, 179 (2010).
14. C. Hsu *et al*, ICRC, HE2.3, 0679 (2011).
15. J.A. Aguilar *et al*, *Nucl. Instrum. Methods* A **675**, 56 (2012).
16. S. Mangano *et al*, *Nucl. Instrum. Methods* A **581**, 695 (2007).
17. S. Biagi *et al*, arXiv:1303.2015 (2013).
18. R. Crocker and F. Aharonian, arXiv:1008.2658v4 (2011).
19. S. Adrian-Martinez *et al*, arXiv:1302.6516 (2013).
20. M.G. Aartsen *et al*, arXiv:1212.4097 (2013).
21. T. Tanaka *et al*, *Astrophys. J.* **742**, 78 (2011).
22. S. Adrian-Martinez *et al*, *Astropart. Phys.* **35**, 552 (2012).
23. S. Adrian-Martinez *et al*, *Phys. Lett.* **B714**, 224 (2012).
24. P. Adamson *et al*, *Phys. Rev. Lett.* **101**, 131802 (2008).
25. J.A. Aguilar *et al*, *Astropart. Phys.* **34**, 652 (2011).
26. J.A. Aguilar *et al*, *Astropart. Phys.* **34**, 539 (2011).
27. J.A. Aguilar *et al*, *Nucl. Instrum. Methods* A **626**, 128 (2011).
28. S. Adrian-Martinez *et al*, *Astropart. Phys.* **35**, 634 (2012).
29. G.E. Pavalas, *Rom. Rep. Phys.* **64**, 325 (2012).